Jeb S. Orr,[1] Arion Kennedy,[1] Emily K. Anderson-Baucum,[1] Corey D. Webb,[1] Steve C. Fordahl,[2] Keith M. Erikson,[2] Yaofang Zhang,[3] Anders Etzerodt,[4] Søren K. Moestrup,[4] and Alyssa H. Hasty[1]

Obesity Alters Adipose Tissue Macrophage Iron Content and Tissue Iron Distribution

Adipose tissue (AT) expansion is accompanied by the infiltration and accumulation of AT macrophages (ATMs), as well as a shift in ATM polarization. Several studies have implicated recruited M1 ATMs in the metabolic consequences of obesity; however, little is known regarding the role of alternatively activated resident M2 ATMs in AT homeostasis or how their function is altered in obesity. Herein, we report the discovery of a population of alternatively activated ATMs with elevated cellular iron content and an iron-recycling gene expression profile. These iron-rich ATMs are referred to as MFe^{hi}, and the remaining ATMs are referred to as MFe^{lo}. In lean mice, ~25% of the ATMs are MFe^{hi}; this percentage decreases in obesity owing to the recruitment of MFe^{lo} macrophages. Similar to MFe^{lo} cells, MFe^{hi} ATMs undergo an inflammatory shift in obesity. In vivo, obesity reduces the iron content of MFe^{hi} ATMs and the gene expression of iron importers as well as the iron exporter, ferroportin, suggesting an impaired ability to handle iron. In vitro, exposure of primary peritoneal macrophages to saturated fatty acids also alters iron metabolism gene expression. Finally, the impaired MFe^{hi} iron handling coincides with adipocyte iron overload in obese mice. In conclusion, in obesity, iron distribution is altered both at the cellular and tissue levels, with AT playing a predominant role in this change. An increased availability of fatty acids during obesity may contribute to the observed changes in MFe^{hi} ATM phenotype and their reduced capacity to handle iron.

Diabetes 2014;63:421–432 | DOI: 10.2337/db13-0213

Obesity is marked by the preferential accumulation of inflammatory M1 adipose tissue (AT) macrophages (ATMs), which play an important role in the development of AT inflammation and insulin resistance (IR) (1). The onset of AT dysfunction has important implications systemically, as AT inflammation and dysregulated lipolysis both promote ectopic lipid deposition and the accompanying metabolic consequences (2). Not surprisingly, a vast majority of the current literature is focused on mechanisms contributing to the recruitment and M1 polarization of infiltrating ATMs. Unfortunately, there remains a paucity of information regarding the physiological role of resident M2 polarized ATMs, as well as the manner by which resident ATM function is compromised in obesity. This represents an important gap in our current understanding of AT physiology, as defining the contribution of resident ATMs to AT homeostasis is a crucial step toward identifying the mechanisms underlying AT dysfunction in obesity.

Recently, the area of AT iron metabolism has received increasing attention. Adipogenesis, which is associated with the upregulation of various genes involved in iron metabolism (3), is induced by heme-iron through

[1]Department of Molecular Physiology and Biophysics, Vanderbilt University School of Medicine, Nashville, TN
[2]Department of Nutrition, University of North Carolina at Greensboro, Greensboro, NC
[3]Department of Pathology, Microbiology and Immunology, Vanderbilt University School of Medicine, Nashville, TN
[4]Department of Biomedicine, Aarhus University, Aarhus, Denmark

Corresponding author: Alyssa H. Hasty, alyssa.hasty@vanderbilt.edu.

Received 6 February 2013 and accepted 8 October 2013.

This article contains Supplementary Data online at http://diabetes.diabetesjournals.org/lookup/suppl/doi:10.2337/db13-0213/-/DC1.

a REV-ERBα–mediated pathway (4,5). Interestingly, whereas iron overload induces adipocyte IR (6,7), strategies to reduce systemic iron concentrations (e.g., low-iron diet, chelation therapy, and phlebotomy) improve insulin sensitivity in obese animal models (8–10) and humans (6,11–13). The aforementioned evidence, combined with the fact that macrophages, as part of the reticuloendothelial system, play the predominant role in systemic iron recycling (14), raises the possibility that ATM iron handling contributes to AT homeostasis.

In the context of iron metabolism, macrophages are most commonly associated with their role in iron recycling for the purpose of providing an adequate supply of iron to support erythropoiesis, as well as to sequester iron as a bacteriostatic measure in response to acute infection (14). Recent data demonstrating that in vitro polarization dictates macrophage iron handling (15,16), combined with the increased M1 polarization observed in obesity, prompted us to explore the potential for ATMs to handle iron. Herein, we report the discovery of a population of alternatively activated resident ATMs that are natively ferromagnetic due to an elevated intracellular iron pool and display an iron-recycling gene expression profile. Additionally, we describe the influence of high-fat feeding on ATM iron handling and provide evidence for a systemic redistribution of tissue iron stores in obesity.

RESEARCH DESIGN AND METHODS

Mice and Diets

Animal care and experimental procedures were performed in accordance with and approval by the Vanderbilt University Institutional Animal Care and Use Committee. Male C57BL/6J wild-type (WT) mice were purchased from The Jackson Laboratory (Bar Harbor, ME). At 8 weeks of age, mice were kept on a normal chow diet (NCD) or placed on low-fat (LFD) (10% kcal from fat, cat. no. D12450B; Research Diets) or high-fat (HFD) (60% kcal from fat, cat. no. D12492; Research Diets) diets for 16 weeks. The LFD and HFD both contain 10 g mineral mix (cat. no. S10026; Research Diets) per 4,000 kcal digestible energy, with each 10 g mineral mix providing 37 mg iron. Mice had free access to food and water throughout the study.

SVF Isolation

Mice were killed via cervical dislocation and perfused with PBS. Epididymal fat pads were removed, and the stromal vascular fraction (SVF) and adipocytes were isolated via collagenase digestion and differential centrifugation as previously described (17,18).

Magnetic Cell Sorting

Cells of the SVF were passed through an autoMACS magnetic-activated cell-sorting system (Miltenyi Biotec) to isolate natively ferromagnetic ATMs. After magnetic separation, nonferromagnetic and ferromagnetic fractions of the SVF were centrifuged at 500*g* for 10 min at 4°C and resuspended in fluorescence-activated cell sorter (FACS) buffer.

FACS Analysis and Sorting

The SVF was labeled with primary fluorophore-conjugated antibodies as previously described, and FACS analysis was performed on an LSRFortessa flow cytometer (BD Biosciences). Data were analyzed and figures generated using Cytobank (19). Isolation of MFe^{hi} and MFe^{lo} ATMs ($F4/80^{hi}CD11b^{hi}$) was performed using a FACSAria III cell sorter (BD Biosciences). The following antibodies, along with appropriate isotype controls, were used to characterize ATM populations: allophycocyanin-conjugated anti-mouse F4/80 (eBioscience), fluorescein isothiocyanate–conjugated anti-mouse CD11b (eBioscience), PE-conjugated anti-mouse CD206 (R&D Systems), phycoerythrin-conjugated anti-mouse MGL1/2 (R&D Systems), phycoerythrin-conjugated anti-mouse CD11c (eBioscience), phycoerythrin-conjugated anti-mouse CCR2 (R&D Systems), and CF594 (Biotium) conjugated anti-mouse CD163.

PKH26 Studies

Male C57BL/6 mice were placed on a 60% HFD for 6 weeks, injected with 5 μmol/L PKH26 i.p., and maintained on HFD for an additional week. Approximately 90% of ATMs label with PKH26 (data not shown). At sacrifice, SVF cells were isolated and stained with allophycocyanin-conjugated anti-mouse F4/80 and DAPI. $F4/80^{+}PKH26^{+}DAPI^{-}$ and $F4/80^{+}PKH26^{-}DAPI^{-}$ macrophages were separated via FACS. Sorted cells were then further separated into MFe^{lo} and MFe^{hi} fractions using the Miltenyi AutoMacs sorter. Cell number in each fraction was determined by counting on a hemocytometer.

Primary Peritoneal Macrophage Isolation and Fatty Acid Treatments

Primary peritoneal macrophages (PPMs) were isolated from mice 3 days after injection with 2% thioglycollate. Cells were plated for 48 h followed by treatment with 500 μmol/L palmitic or oleic acid for 24 h as previously described (20). Cells were collected in TRIzol reagent for RNA isolation and real-time RT-PCR analysis.

RNA Isolation and Real-Time RT-PCR

RNA was isolated from liver using an RNeasy mini-kit (Qiagen) and from adipocytes and ATMs using TRIzol reagent (Invitrogen) according to the manufacturer's instructions with minor modifications, including the use of 1-bromo-3-chloropropane (Sigma-Aldrich) and RNase-free glycogen (Roche Diagnostics). Additionally, RNA extracted from isolated adipocytes and ATMs was subjected to DNase treatment (DNA-free kit; Applied Biosystems). cDNA was synthesized using the iScript cDNA synthesis kit (BioRad), and real-time RT-PCR was performed on an iQ5 cycler (BioRad) using Taqman gene expression assays (Applied Biosystems [cat. nos. available upon request]). Gene expression for MFe^{hi} and

MFe^{lo} cells was normalized to hypoxanthine guanine phosphoribosyl transferase or glyceraldehyde-3-phosphate dehydrogenase using the $2^{-\Delta\Delta Ct}$ method (21). Expression for PPMs was normalized to cytochrome b.

Tissue Iron Visualization

Tissue iron distribution was visualized using the perfusion Perls' Prussian blue staining method (22). Subsequent to perfusion with PBS supplemented with heparin (5 units/mL), mice were perfused with a Prussian blue staining solution containing 4% paraformaldehyde, 1% potassium ferrocyanide, and 1% HCl. One hour postperfusion, tissues were removed and incubated in staining solution for 12 h at 4°C prior to being paraffin embedded. Tissue sections were then cleared, hydrated, and counterstained with nuclear fast red.

Cellular and Tissue Iron Quantification

Ferromagnetic and nonferromagnetic ATMs were digested in ultra-pure HNO_3. A double-focusing sector field high-resolution inductively coupled plasma mass spectrometry (ICP-MS) (ELEMENT II; Thermo Fisher Scientific, Bremen, Germany) equipped with ESI auto sampler was used for the quantitative analysis of ATM iron content in the isolated cells. The elemental measurement was performed on isotopes ^{25}Mg, ^{42}Ca, ^{55}Mn, ^{56}Fe, ^{59}Co, ^{60}Ni, ^{63}Cu, and ^{66}Zn at a mass resolution $m/\Delta m$ 4,400 to separate molecular interferences. Elemental standards for external calibration were purchased from Fluka.

Splenic, hepatic, and adipocyte iron concentrations were measured with graphite furnace atomic absorption spectrometry (Varian AA240; Varian). Spleen and liver samples were homogenized in radioimmunoprecipitation assay buffer 1:10 w/v for protein determination using the bicinchoninic assay (Pierce Chemicals). An aliquot of the homogenate was then digested in ultra-pure HNO_3 (1:3 v/v dilution) for 48–72 h at 60°C in a sand bath. Adipocyte pellets were homogenized in 100 μL radioimmunoprecipitation assay for bicinchoninic assay

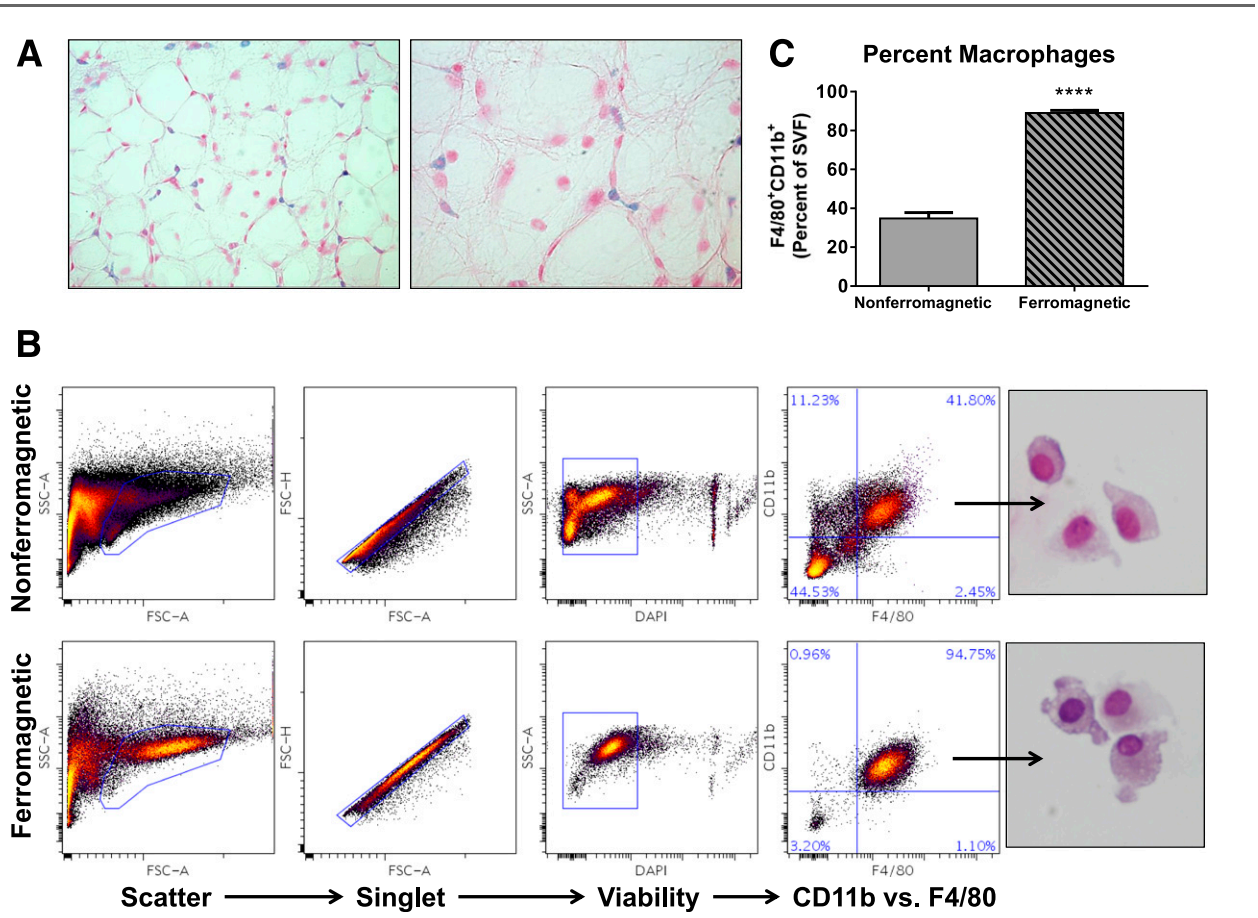

Figure 1—AT contains a population of ferromagnetic ATMs. *A*: Identification of iron-rich ATMs in epididymal fat pads of NCD mice (*left panel*, ×20, and *right panel*, ×40 magnification). Mice were perfused with Perls' Prussian blue staining solution, and sections were counterstained with nuclear fast red. Iron-containing ATMs are stained blue. *B*: Characterization of ferromagnetic and nonferromagnetic fractions of the SVF from NCD mice by flow cytometry. After magnetic sorting, the proportion of viable ATMs ($F4/80^{hi}CD11b^{hi}$) within ferromagnetic and nonferromagnetic fractions was quantified. The *rightmost column* depicts diff-quick staining of isolated ATMs from each fraction. *C*: Comparison of ATMs as a percentage of viable cells in the nonferromagnetic and ferromagnetic fractions of the SVF from NCD mice (n = 13/group). ****$P < 0.0001$. FSC, forward scatter.

protein analysis, and aliquots were digested in 1:2 v/v ultra-pure HNO_3. All digested samples were further diluted with a 2% nitric acid solution (1:20 to 1:100, as necessary) for analysis. Bovine liver (National Bureau of Standards, Standard Reference Material, United States Department of Commerce, Washington, DC) (184 μg Fe/g) was used as an internal standard for analysis.

Serum Iron Parameters

Total iron-binding capacity and serum iron, transferrin, and ferritin concentrations were quantified using an ACE Alera clinical chemistry system (Alfa Wasserman). Transferrin saturation was calculated as (serum iron/total iron-binding capacity) × 100%.

Statistics

All data are reported and presented in figures as means ± SEM. Two-tailed unpaired *t* tests were used to compare means between two groups, and one-way ANOVA with the Tukey correction for multiple comparisons was used when comparing more than two groups. Statistical analyses were performed using GraphPad Prism (La Jolla, CA).

RESULTS

AT Contains a Population of Ferromagnetic Macrophages

A population of iron-containing ATMs distributed interstitially throughout the AT of lean, NCD-fed male WT mice was detected using the perfusion Perls' Prussian blue method (22) (Fig. 1*A*). This population was isolated from the SVF via magnetic column separation, yielding a ferromagnetic population and a nonferromagnetic population. Subsequent FACS using F4/80 and CD11b (Fig. 1*B*) demonstrated that 35% of nonferromagnetic cells were macrophages (Fig. 1*C*), compared with 90% of ferromagnetic cells. Unless otherwise indicated, subsequent experiments used a strategy of sequential magnetic/FACS to permit the direct comparison of viable ferromagnetic (MFe^{hi}) and nonferromagnetic (MFe^{lo}) ATMs. MFe^{hi} ATMs displayed a greater than twofold increase in cellular iron content compared with MFe^{lo} ATMs (Fig. 2*A*). For confirmation that the ferromagnetic properties of the MFe^{hi} cells were due to increased iron content as opposed to other ferromagnetic elements, ICP-MS was used to assess nickel and cobalt. In addition, copper, zinc, magnesium, calcium, and manganese were quantified (Supplementary Fig. 1). Only iron concentrations were significantly different between the MFe^{hi} and MFe^{lo} cells.

In addition to an elevated iron pool, MFe^{hi} ATMs exhibited a gene expression profile indicating a role in iron recycling (Fig. 2*B*). This included significantly greater expression of the genes involved in iron uptake (*Cd163* and transferrin receptor-1 [*Tfrc*]), metabolism (heme oxygenase-1 [*Hmox1*]), storage (ferritin light and heavy chains [*Ftl1* and *Fth1*, respectively]), and export

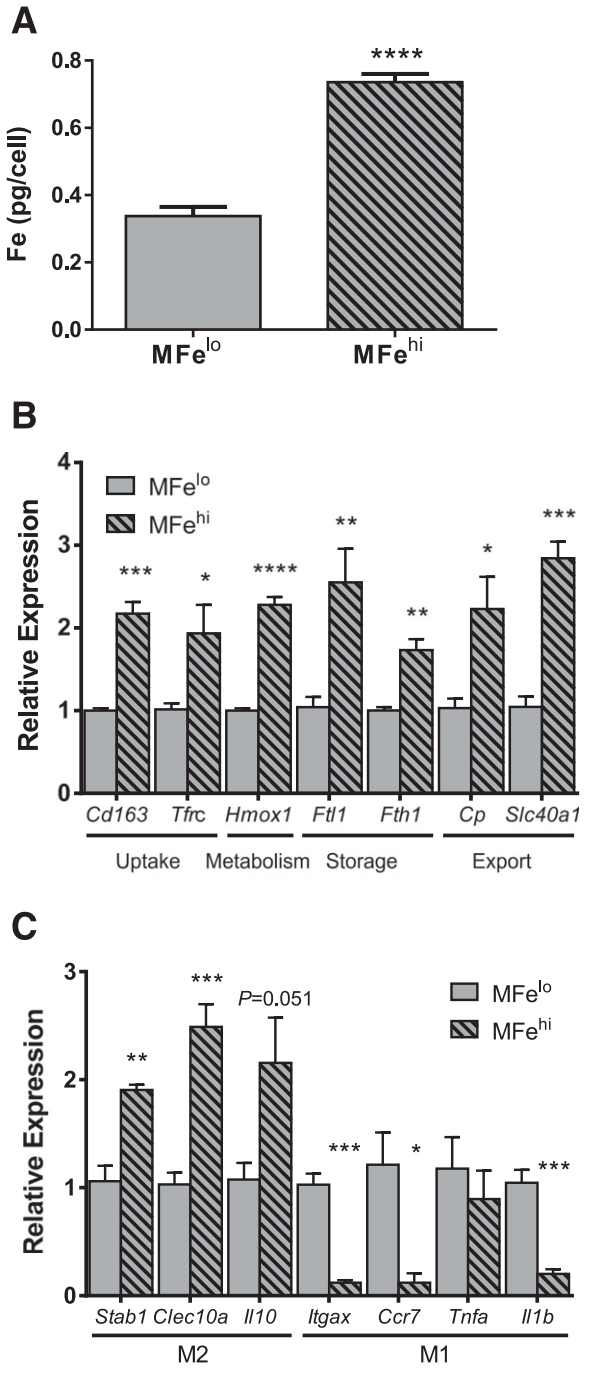

Figure 2—MFe^{hi} ATMs are a subset of alternatively activated ATMs with elevated cellular iron content and an iron-recycling gene expression profile. *A*: Comparison of MFe^{lo} and MFe^{hi} ATM iron content from NCD-fed mice. MFe^{lo} and MFe^{hi} ATMs were isolated via sequential magnetic and FACS sorting, and cellular iron content was quantified by ICP-MS (n = 4/group) (****P < 0.0001). *B* and *C*: Comparison of MFe^{lo} and MFe^{hi} ATM gene expression. MFe^{lo} and MFe^{hi} ATMs were isolated from NCD-fed mice and analyzed by real-time RT-PCR for the expression of genes involved in iron metabolism (*B*) and markers of M2 and M1 polarization (*C*) (n = 3–4/group). *P < 0.05, **P < 0.01, ***P < 0.001, ****P < 0.0001.

(ceruloplasmin [*Cp*] and ferroportin-1 [*Slc40a1*]) in MFe^{hi} compared with MFe^{lo} cells. The upregulation of transferrin receptor and CD163, the hemoglobin-scavenger receptor, implicate uptake of iron by MFe^{hi} cells from various sources.

MFe^{hi} Are Alternatively Activated

In light of recent data suggesting that M2 polarization induces an iron recycling phenotype (15), we sought to determine the polarization of MFe^{hi} ATMs. While all ATMs from lean AT are expected to be M2-like (23), the

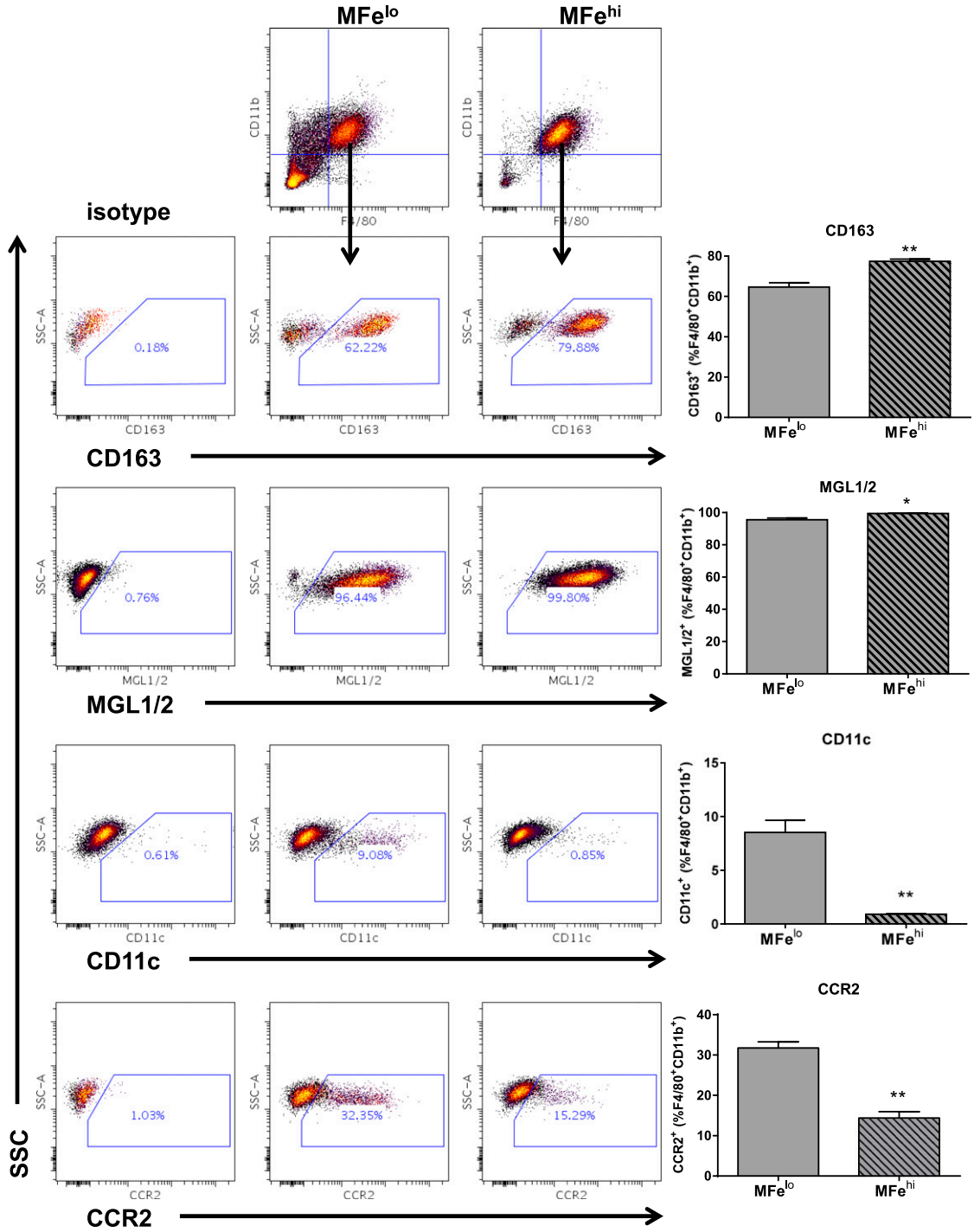

Figure 3—FACS analysis of MFe^{lo} and MFe^{hi} ATMs. Flow cytometry was used to measure MFe^{lo} and MFe^{hi} ATM expression of M2 markers (CD163 and MGL1/2) and M1 markers (CD11c and CCR2) from the SVF of NCD mice. The *top row* depicts the initial gating on viable F4/80^{hi}CD11b^{hi} MFe^{lo} and MFe^{hi} ATMs. Isotype controls used to gate for M2 and M1 markers are shown in the *left column*. The *rightmost column* compares the number of MFe^{lo} and MFe^{hi} ATMs positive for each M2 or M1 marker as a percent of viable F4/80^{hi}CD11b^{hi} ATMs (n = 3–4/group for each marker). *P < 0.05, **P < 0.01.

expression of M2 markers, stabilin-1 (*Stab1*), macrophage galactose-type C-type lectin 1 (MGL1 [*Clec10a*]), and IL-10 (*Il10*) were significantly increased in MFe^{hi} compared with MFe^{lo} ATMs. In contrast, the M1 markers, CD11c (*Itgax*), CCR7 (*Ccr7*), and Il-1β (*Il1b*) were significantly reduced in MFe^{hi} cells (Fig. 2*C*). Flow cytometry also revealed that a significantly greater proportion of MFe^{hi} ATMs are CD163 and MGL1/2 positive, whereas a significantly reduced proportion of MFe^{hi} ATMs express the M1 markers, CD11c and CCR2 (Fig. 3).

Obesity Induces a Shift in MFe^{hi} Polarization Toward an Inflammatory M1 Phenotype

Next, mice were placed on an LFD or HFD for 16 weeks to determine the impact of obesity on the polarization and iron-handling phenotype of MFe^{hi} ATMs. As anticipated, HFD feeding increased the absolute number of ATMs (Fig. 4*A*), as well as the number of ATMs relative to AT mass (Fig. 4*B*). This increase was driven by a dramatic accumulation of MFe^{lo} ATMs, whereas the relative number of MFe^{hi} ATMs did not change after HFD. The marked accumulation of MFe^{lo} ATMs resulted in a significant decrease in the number of MFe^{hi} ATMs as a percent of total ATMs from 27% in lean controls to 14% in obese mice (Fig. 4*C*). Perls' Prussian blue staining of AT revealed that MFe^{hi} ATMs are predominately, but not exclusively, located interstitially, with a small number associated with crown-like structures within obese AT (Supplementary Fig. 2). In agreement with the previously demonstrated inflammatory nature of recruited ATMs, MFe^{lo} ATMs isolated from obese mice display decreased gene expression of M2 markers and increased expression of M1 markers compared with MFe^{lo} ATMs from lean mice (Supplementary Fig. 3*A*). Despite retaining an alternatively activated gene expression profile relative to MFe^{lo} ATMs from obese mice (Supplementary Fig. 3*B*), HFD-fed compared with LFD-fed mice had decreased MFe^{hi} ATM gene expression of the M2 markers, *Stab1* and *Clec10a* (Fig. 4*D*). The MFe^{hi} ATM population also exhibited an inflammatory shift, as HFD feeding increased *Itgax, Ccr7, Tnfα*, and *Il1β* expression by MFe^{hi} ATMs. As expected, flow cytometric analysis of MFe^{lo} cells demonstrated an increased M1-like profile in cells from HFD-fed mice (Supplementary Fig. 4). This shift was also noted in MFe^{hi} ATMs. Flow analysis indicated a decrease in MGL1/2 and CD206 expression in obese MFe^{hi} ATMs

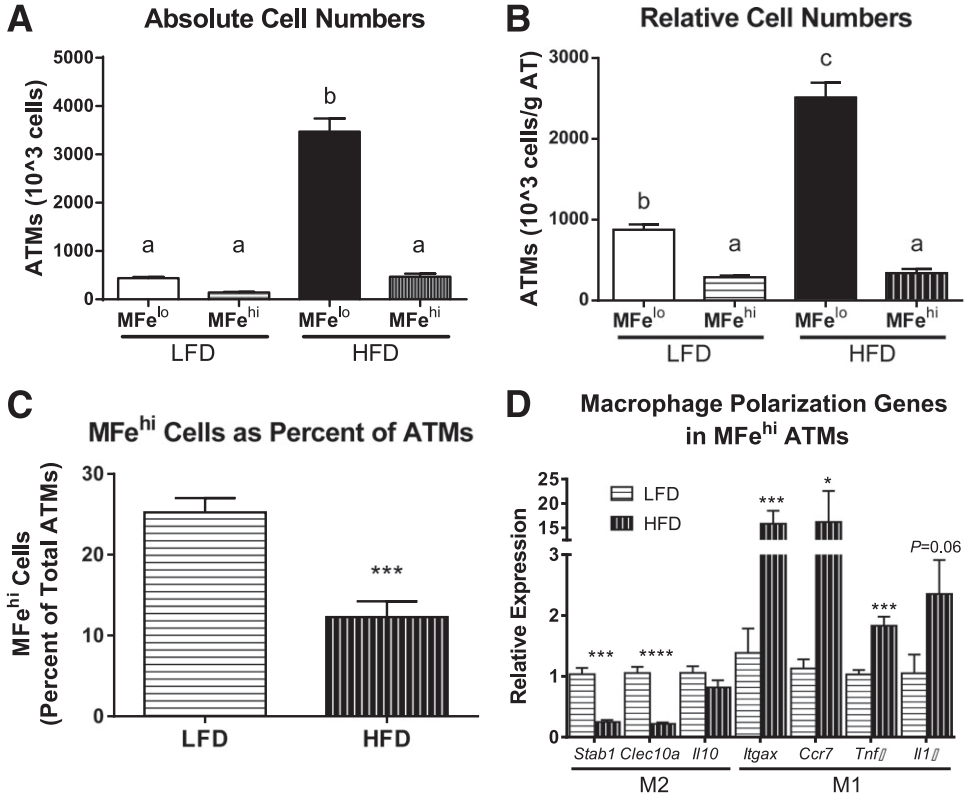

Figure 4— MFe^{hi} ATMs do not accumulate in obesity but do transition toward an inflammatory M1 polarization. *A* and *B*: The number of MFe^{lo} ATMs are increased on an absolute basis (*A*) and relative to epididymal fat pad mass (*B*) in HFD compared with LFD mice (n = 9/group) ($P < 0.05$ for groups not connected by the same letter). *C*: The increase in MFe^{lo} ATMs in HFD mice leads to a reduction in the number of MFe^{hi} ATMs as a percent of total ATMs (n = 9/group) (***$P < 0.001$). *D*: MFe^{hi} ATM phenotype shifts toward an inflammatory M1 polarization in obesity. After sequential magnetic and FACS sorting, mRNA expression of M2 and M1 markers by MFe^{hi} ATMs isolated from LFD and HFD mice was analyzed via real-time RT-PCR (n = 4–7/group). *$P < 0.05$, ***$P < 0.001$, ****$P < 0.0001$.

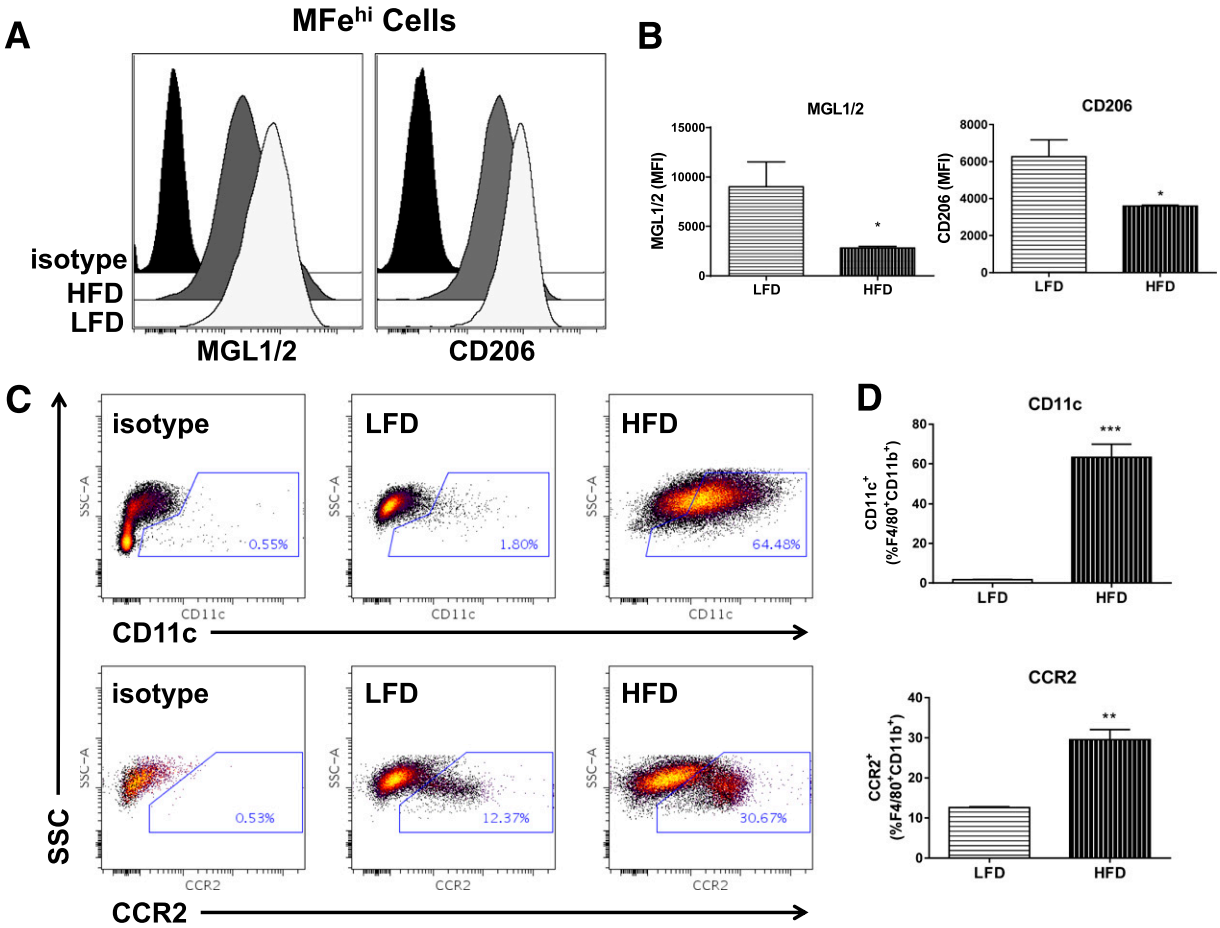

Figure 5—Obesity induces an inflammatory shift in MFe^{hi} ATM polarization. *A*: MFe^{hi} ATM expression of M2 markers, MGL1/2 (*left panel*) and CD206 (*right panel*), is reduced in obesity. M2 marker expression by viable F4/80^{hi}CD11b^{hi}, MFe^{hi} ATMs was measured by flow cytometry. Isotype controls, HFD MFe^{hi} ATMs, and LFD MFe^{hi} ATMs are represented by black, gray, and white histograms, respectively. *B*: Quantification and comparison of MGL1/2 (*left panel*) and CD206 (*right panel*) expression by LFD and HFD MFe^{hi} ATMs (n = 3/group for each marker) (*P < 0.05). *C*: Obesity increases the proportion of MFe^{hi} ATMs expressing the M1 markers CD11c (*top row*) and CCR2 (*bottom row*). M1 marker expression by viable F4/80^{hi}CD11b^{hi}, MFe^{hi} ATMs was measured by flow cytometry. Representative FACS plots of isotype controls, LFD MFe^{hi} ATMs, and HFD MFe^{hi} ATMs are shown in the *left*, *middle*, and *right columns*, respectively. *D*: Quantification and comparison of the number of CD11c^{+} (*top panel*) and CCR2^{+} (*bottom panel*) MFe^{hi} ATMs as a percent of total viable F4/80^{hi}CD11b^{hi}, MFe^{hi} ATMs in LFD and HFD mice (n = 3/group for each marker). *P < 0.05, **P < 0.01, ***P < 0.001.

(Fig. 5*A* and *B*) and a significant increase in the proportion of MFe^{hi} ATMs expressing CD11c and CCR2 (Fig. 5*C* and *D*).

Obesity Impairs MFe^{hi} Iron Handling

The inflammatory shift observed by MFe^{hi} ATMs after HFD was associated with a significant reduction in iron content (Fig. 6*A*). This effect was restricted to MFe^{hi} ATMs, as high-fat feeding did not significantly influence MFe^{lo} ATM iron content. Interestingly, the inclusion of ATM iron data from NCD mice in our analysis revealed that MFe^{hi} ATMs from NCD and LFD mice possess similar iron content, as do MFe^{lo} ATMs from all three groups (Supplementary Fig. 5*A*). The impairment in MFe^{hi} ATM iron handling after HFD was apparent at the transcriptional level as well. High-fat feeding resulted in decreased MFe^{hi} ATM expression of genes involved in iron uptake, metabolism, storage, and export (Fig. 6*B*). Obesity produced similar relative changes in the expression of iron-handling genes by MFe^{lo} ATMs (Supplementary Fig. 3*A*).

For determination of a potential mechanism by which obesity alters macrophage iron handling, mouse PPMs were treated with 500 μmol/L palmitate or oleate (Fig. 6*C*). As expected, palmitate increased inflammatory genes such as *Tnfα* and *Il6*, while oleate increased M2 markers such as *Clec10a* and *Cd163*. Interestingly, expression of *Ftl1* and *Fth1* and the protein levels of hemoxygenase-1 were reduced in palmitate- but not oleate-treated PPMs. Expression of *Slc40a1* was not altered by treatment with either fatty acid (data not shown). These studies indicate that saturated fatty acids released from IR adipocytes in obesity may contribute to the impaired macrophage iron handling observed during HFD feeding.

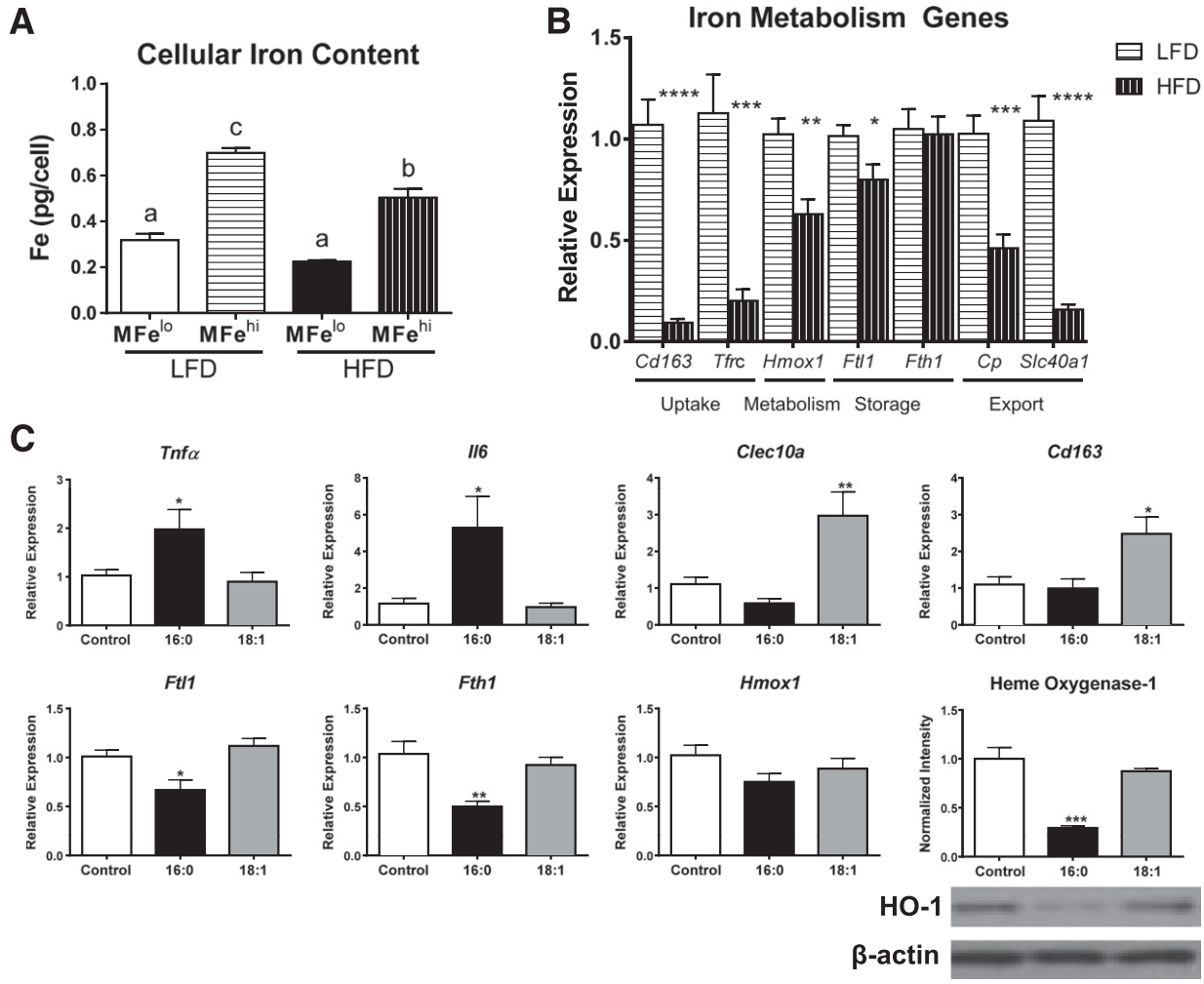

Figure 6—Obesity impairs MFe^{hi} iron handling. *A*: Comparison of MFe^{lo} and MFe^{hi} ATM iron content from LFD and HFD mice. MFe^{lo} and MFe^{hi} ATMs were isolated via sequential magnetic and FACS sorting, and cellular iron content was quantified by ICP-MS (n = 5–6/group) (*P < 0.05 for groups not connected by the same letter). *B*: Obesity reduces MFe^{hi} ATM iron metabolism gene expression. MFe^{hi} ATMs were isolated from LFD and HFD mice and analyzed by real-time RT-PCR for the expression of genes involved in iron metabolism (n = 5–7/group) (*P < 0.05, **P < 0.01, ***P < 0.001, ****P < 0.0001). *C*: PPMs were cultured with 500 μmol/L palmitic acid (16:0) or oleic acid (18:1) for 24 h. RNA was isolated, and gene expression for *Tnfα, Il6, Clec10a, Cd163, Ftl1*, *Fth1,* and *Hmox1* was performed. In addition, Western blotting for hemoxygenase-1 was performed. Data are presented as the mean ± SEM for 4–6 samples per group. *P < 0.05, **P < 0.01, ***P < 0.001.

Macrophages Recruited During HFD Feeding Are MFe^{lo}

The identical number of MFe^{hi} ATMs relative to AT mass observed in LFD- and HFD-fed mice suggests that recruited macrophages do not take on a role in iron metabolism. To test this hypothesis, PKH26 labeling studies were performed. Mice were fed HFD for 6 weeks and then injected with PKH26 to label preexisting ATMs. One week after injection, the SVF was collected and sorted to isolate F4/80^{+}PKH^{+} (pre-existing) and F4/80^{+}PKH^{-} (newly recruited) ATMs. Subsequently, magnetic sorting was used to quantify the proportion of MFe^{hi} and MFe^{lo} ATMs in each fraction (Fig. 7). Of the total cells counted, 60% were PKH^{+}MFe^{lo} and 13% were PKH^{+}MFe^{hi}, indicating that both MFe^{lo} and MFe^{hi} cells labeled with PKH were retained in the AT. Newly recruited PKH^{-}MFe^{lo} cells made up 26% of the total ATMs. In contrast, only 0.2% of the PKH^{-} cells were MFe^{hi}, indicating that recruited macrophages do not take on an MFe^{hi} phenotype.

Impaired MFe^{hi} Iron Handling Coincides With Adipocyte Iron Accumulation and Hepatic Iron Deficiency in Obesity

Despite the reduction in MFe^{hi} ATM iron content after HFD feeding, staining for tissue iron accumulation via perfusion Perls' Prussian blue indicated that whole AT iron concentrations were increased in obesity (Fig. 8*A*). Interestingly, HFD feeding produced a fourfold increase in adipocyte iron concentration (Fig. 8*B*), as well as a gene expression profile consistent with iron accumulation (Fig. 8*C*). In addition to iron accumulation, adipocytes isolated from obese AT displayed an

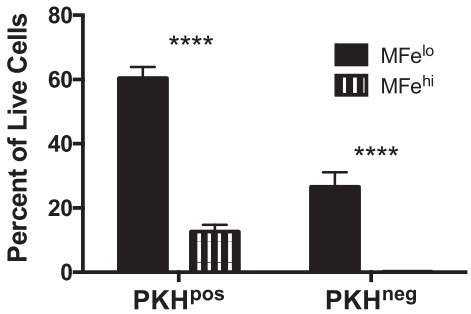

Figure 7—ATMs recruited during HFD feeding are MFe^{lo}. Mice were fed an HFD for 6 weeks and then injected with PKH26 to label preexisting ATMs. Mice were maintained on the HFD for an additional week so that circulating monocytes could be recruited to the AT. Mice were killed, and the SVF was collected by collagenase digestion. ATMs were collected by FACS for F4/80 and were separated as either PHK^{pos} (preexisting) or PKH^{neg} (newly recruited). MFe^{lo} and MFe^{hi} cells were then isolated by magnetic sorting and counted. Data are presented as the percent of live cells. Almost no PKH^{-} MFe^{hi} cells were detected, indicating that newly recruited cells do not immediately take on a role in iron metabolism. Data are presented as the mean ± SEM for 7 samples per group. $^{****}P < 0.0001$.

inflammatory shift in gene expression, including decreased *Adipoq* expression, upregulation of *Il6*, and a trend for increased *Tnfα* expression (Fig. 8*D*).

Importantly, our finding of adipocyte iron overload in obesity was not indicative of a global increase in tissue iron stores, as Perls' Prussian blue staining and quantification of liver iron concentrations revealed a >50% reduction in obese mice compared with lean controls (Fig. 8*E* and *F*). Interestingly, this change in liver iron status did not elicit significant changes in the expression of genes associated with cellular iron handling (Fig. 8*G*); however, obesity reduced the expression of a specific cluster of genes important to the regulation of systemic iron homeostasis, including *Trfr2* (transferrin receptor 2), *Bmp6* (bone morphogenic protein 6), *Tmprss6* (transmembrane protease, serine 6), and *Hamp1* (hepcidin) (Fig. 8*H*). In contrast to the changes observed in hepatic and adipocyte iron concentrations, splenic iron concentrations were not significantly altered in obese mice, further pointing to a selective repartitioning of tissue iron stores in obesity (Supplementary Fig. 5*B* and *C*).

With regard to circulating iron parameters, serum iron concentrations were not influenced by obesity (Supplementary Table 1). In contrast, serum transferrin was significantly elevated following high-fat feeding, which is consistent with the hepatic iron deficiency observed in obese mice. Circulating ferritin concentrations were likewise increased in obese mice.

DISCUSSION

The past decade has witnessed a dramatic increase in our understanding and appreciation of the manner in which ATMs contribute to the metabolic consequences of obesity. Although the primary emphasis of the current literature lies with the contribution of ATMs to AT inflammation and IR, various studies have directly implicated ATMs in a number of homeostatic roles, including lipolysis (24), AT development (25), and remodeling (26). The current study demonstrates that resident ATMs are also involved in iron metabolism and lays the foundation for future investigations regarding a role for ATM iron handling in AT homeostasis, as well as the contribution of dysregulated ATM iron metabolism to AT function in obesity.

In light of the epidemiological evidence linking hyperferritinemia with obesity and related comorbidities (27), several studies have focused on the effects of altered iron metabolism on AT function (10,28) and the possibility that AT may play an active role in regulating systemic iron homeostasis (29,30). However, the potential contribution of ATMs to AT iron metabolism remains an unexplored area of investigation. The current study provides the first evidence that ATMs play a role in local AT iron metabolism and highlights the significant heterogeneity that exists with respect to an ATM iron-handling phenotype. Specifically, that obesity induces a selective decrease in MFe^{hi} ATM iron content and that infiltrating ATMs do not accumulate iron suggest that iron handling within AT is restricted to a discrete population of resident alternatively activated MFe^{hi} ATMs. Importantly, this paradigm is not without precedence, as splenic (i.e., red pulp, marginal zone, and metallophillic macrophages) and atherosclerotic plaque macrophage populations present similarly divergent roles regarding iron metabolism (31,32).

Recent studies describing the in vitro influence of polarization on macrophage iron handling suggest that M2 polarization induces an iron-recycling phenotype characterized by elevated *Tfrc*, *Cd163*, *Hmox*1, and *Fpn* expression and an increased capacity for iron uptake and release (15,16). In contrast, M1 polarization elicits an iron sequestration phenotype. Our in vivo data agree with this model insofar as MFe^{hi} ATMs present an iron-recycling gene expression profile (i.e., upregulation of iron importers and the exporter, ferroportin) and elevated expression of M2 markers. However, important differences exist with respect to MFe^{hi} ATM phenotype and the published in vitro model of M1/M2 macrophage polarization and iron metabolism (15,16). The in vitro model suggests that M2 polarized macrophages have a reduced capacity for iron storage and that M1 macrophages display an iron sequestration phenotype with an associated increase in ferritin heavy-chain expression. This stands in stark contrast to our finding of elevated iron content in alternatively activated MFe^{hi} ATMs. Likewise, based on the published model, one would predict that inflammation would lead to iron sequestration by M1 ATMs. On the contrary, our in vivo data suggest that obesity-associated inflammation does not increase recruited M1 ATM iron stores; rather, we observed a selective decrease in the iron content of MFe^{hi} ATMs coinciding with a shift toward an inflammatory

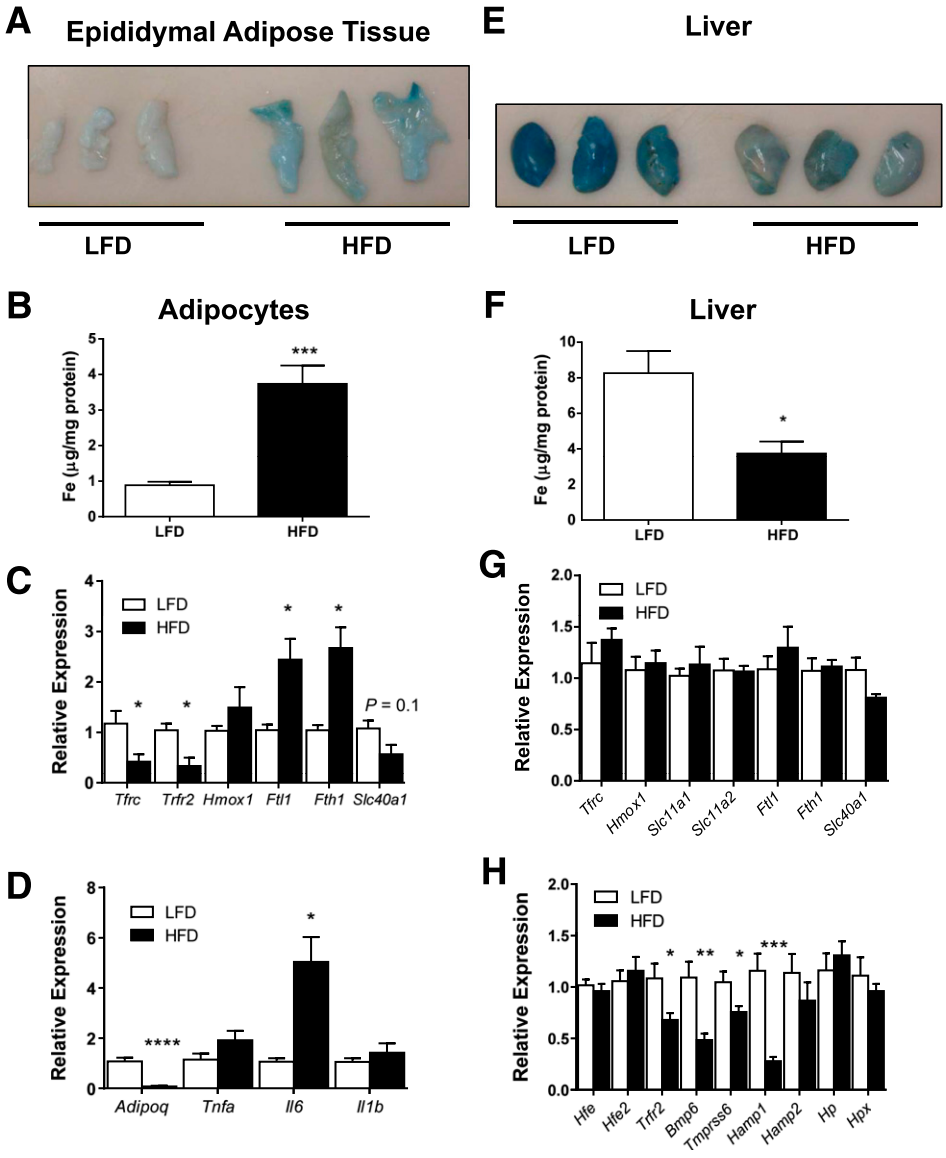

Figure 8—Obesity induces tissue iron repartitioning. *A*: Visual comparison of epididymal fat pad iron content between LFD and HFD mice. Mice were perfused with Perls' Prussian blue staining solution, and tissues were removed 1 h postperfusion. *B*: Comparison of adipocyte iron concentrations between LFD and HFD mice. Adipocytes were isolated from the epididymal fat pads of LFD and HFD mice via collagenase digestion. Adipocyte iron content was quantified by atomic absorption spectrometry and expressed relative to total protein (n = 6–7/group) (***$P < 0.001$). *C* and *D*: Comparison of adipocyte gene expression from LFD and HFD mice. Real-time RT-PCR was used to assess adipocyte mRNA expression of genes involved in cellular iron metabolism (*C*) and *Adipoq* (adiponectin) and inflammatory cytokines (*D*). *E*: Visual comparison of hepatic iron content between LFD and HFD mice. Comparably sized pieces of the left lobe are presented. *F*: Comparison of hepatic iron concentrations between LFD and HFD mice. Liver iron content was quantified via atomic absorption spectrometry and expressed relative to total protein (n = 5/group) (*$P < 0.05$). *G* and *H*: Comparison of liver gene expression from LFD and HFD mice. Real-time RT-PCR was used to assess hepatic mRNA expression of genes involved in cellular (*G*) and systemic (*H*) iron metabolism (n = 4–7/group). *$P < 0.05$, **$P < 0.01$, ***$P < 0.001$, ****$P < 0.0001$.

phenotype. Furthermore, our studies demonstrate that treatment of macrophages with saturated fatty acids reduced genes and proteins associated with iron storage. Thus, it is possible that macrophage inflammation induced by fatty acids invokes different effects on iron metabolism compared with M1 polarization via traditional methods. Although the above discrepancies do not necessarily preclude the possibility that MFe^{hi} ATMs represent a subset of M2-polarized macrophages (i.e., M2a, -b, or -c) (33), the phenotype of MFe^{hi} ATMs more closely aligns with the recently characterized Mhem polarization state (31). Mhem macrophages are a discrete population of atheroprotective macrophages induced after intraplaque hemorrhage and the resultant heme exposure. Similar to MFe^{hi} ATMs, Mhem macrophages display elevated iron content and increased expression of *Cd163*, *Hmox-1*, and *Il-10*. Interestingly, the Mhem program is driven by heme-induced activating

transcription factor-1 phosphorylation. Further research will be necessary to determine whether the observed MFe^{hi} phenotype is similarly regulated.

Results of the current study raise a number of important questions regarding the physiological relevance of ATM iron metabolism to AT function as well as the mechanism(s) underlying impaired MFe^{hi} ATM iron handling in obesity. Adequate control of iron availability appears crucial to AT homeostasis. Previous in vitro studies have demonstrated that heme-associated iron induces preadipocyte differentiation and is required to support adipogenesis (4,5). In contrast to its role in supporting adipogenesis, in vitro iron treatment induces lipolysis and IR in mature adipocytes (7,34). Furthermore, Gabrielsen et al. (6) recently used an elegant series of dietary and genetic manipulations to induce adipocyte iron overload and demonstrated that adipocyte iron regulates adiponectin expression and systemic glucose homeostasis. In agreement, we observed a significant decrease in adipocyte *Adipoq* gene expression after obesity-induced adipocyte iron accumulation. Interestingly, the occurrence of adipocyte iron overload in our study coincided with a reduction in MFe^{hi} ATM iron content and iron-recycling gene expression. In light of our findings and the available literature regarding AT iron metabolism, we propose a working model whereby resident MFe^{hi} ATMs fulfill the dual roles of providing an adequate supply of iron to support adipogenesis, analogous to macrophages acting as a source of iron for proliferating lymphocytes in the lymph nodes (35), and protecting adipocytes from oxidative stress by scavenging extracellular heme. Thus, impaired MFe^{hi} ATM iron handling in the setting of hyperinsulinemia, which induces adipocyte iron uptake (36,37), may play a role in the development of AT dysfunction in obesity. Future experiments are required to determine the role of resident ATM iron metabolism in AT homeostasis.

An intriguing aspect of the current study includes the observation of tissue iron repartitioning in obesity, which occurred in the absence of changes in serum iron concentrations. Specifically, hepatic iron concentrations were significantly decreased, whereas adipocyte iron concentrations were increased. Our finding of reduced hepatic iron stores and hepcidin expression is in line with previous studies in rodent models of obesity (38–40). Although our in vivo studies were not designed to address the underlying mechanism(s) responsible for changes in iron distribution, our data point to a potentially important interaction between iron and lipid metabolism. After 16 weeks of HFD, WT mice display visceral lipoatrophy accompanied by a dramatic increase in liver lipid accumulation (41). Likewise, high-fat feeding has been shown to induce ATM lipid accumulation (42). Interestingly, our data suggest that ectopic lipid accumulation in obesity is accompanied by a shift in tissue iron distribution, such that adipocytes display iron concentrations equivalent to the liver. Thus, sites crucial to the maintenance of systemic iron homeostasis (i.e., liver and macrophages) experience lipid accumulation coincident with a relative state of iron deficiency. Conversely, dysregulated lipolysis and atrophy of the AT are accompanied by adipocyte iron overload.

Increasing evidence points to important yet complex associations among adiposity, IR, and iron metabolism. The potential contribution of AT to systemic iron homeostasis has received increased attention recently; however, the role of ATMs in AT iron metabolism remains unexplored. The current study describes a novel population of alternatively activated MFe^{hi} ATMs that displays elevated cellular iron content along with an anti-inflammatory and iron-recycling gene expression profile. Importantly, the impairment of MFe^{hi} ATM iron handling is temporally associated with adipocyte iron overload and AT dysfunction in obesity. Additionally, our data provide the first evidence that diet-induced obesity leads to a repartitioning of tissue iron stores and argue for a coordinated regulation of lipid and iron metabolism. Collectively, our data lay the foundation for future investigations regarding the role of ATM iron handling in AT homeostasis and the mechanisms underlying the development of impaired iron metabolism in obesity.

Funding. This project was supported by a Discovery Grant in Innovative Diabetes Research from the Vanderbilt Diabetes Center (DK-20593) and National Institutes of Health (NIH) R21 DK-095456. The authors were supported by the following grants: NIH Ruth L. Kirschstein NRSA F32 DK-091040 (to J.S.O.), American Diabetes Association Mentor–based Postdoctoral Fellowship 7-10-MI-05 (to A.K.), American Heart Association Pre-doctoral Fellowship 12PRE11910047 (to E.K.A.-B.), NIH R21 DK-095456 (to C.D.W. and A.H.H.), and American Heart Association Established Investigator Award 12EIA8270000 (to A.H.H.). Flow cytometry was performed through Vanderbilt University Medical Center (VUMC) Digestive Disease Research Center supported by NIH DK-058404 Core Scholarship. Cellular iron measurements were performed by the VUMC Mass Spectrometry Research Core (supported by NIH Shared Instrumentation grant S10 RR-026742). Immunofluorescence imaging was conducted in part through the use of the VUMC Cell Imaging Shared Resource (supported by NIH grants CA-68485, DK-20593, DK-58404, HD-15052, DK-59637, and EY-08126). Serum iron parameter measurements were performed by the Vanderbilt Translational Pathology Shared Resource (supported by DK-059637).

Duality of Interest. S.K.M. is a minority shareholder of Cytoguide ApS (Aarhus, Denmark). The rat anti-mouse CD163 monoclonal antibody (E10B10) was a kind gift from Cytoguide ApS. No other potential conflicts of interest relevant to this article were reported.

Author Contributions. J.S.O. collected and analyzed data and wrote the manuscript. A.K., E.K.A.-B., C.D.W., S.C.F., K.M.E., Y.Z., A.E., and S.K.M. helped collect data and edit the manuscript. A.H.H. obtained funding, aided with data analysis, and edited the manuscript. A.H.H. is the guarantor of this work and, as such, had full access to all the data in the study and takes responsibility for the integrity of the data and the accuracy of the data analysis.

References

1. Sun K, Kusminski CM, Scherer PE. Adipose tissue remodeling and obesity. J Clin Invest 2011;121:2094–2101

2. Virtue S, Vidal-Puig A. Adipose tissue expandability, lipotoxicity and the metabolic syndrome–an allostatic perspective. Biochim Biophys Acta 2010;1801:338–349
3. Festa M, Ricciardelli G, Mele G, Pietropaolo C, Ruffo A, Colonna A. Overexpression of H ferritin and up-regulation of iron regulatory protein genes during differentiation of 3T3-L1 pre-adipocytes. J Biol Chem 2000;275:36708–36712
4. Chen JJ, London IM. Hemin enhances the differentiation of mouse 3T3 cells to adipocytes. Cell 1981;26:117–122
5. Kumar N, Solt LA, Wang Y, et al. Regulation of adipogenesis by natural and synthetic REV-ERB ligands. Endocrinology 2010;151:3015–3025
6. Gabrielsen JS, Gao Y, Simcox JA, et al. Adipocyte iron regulates adiponectin and insulin sensitivity. J Clin Invest 2012;122:3529–3540
7. Green A, Basile R, Rumberger JM. Transferrin and iron induce insulin resistance of glucose transport in adipocytes. Metabolism 2006;55:1042–1045
8. Cooksey RC, Jones D, Gabrielsen S, et al. Dietary iron restriction or iron chelation protects from diabetes and loss of beta-cell function in the obese (ob/ob lep-/-) mouse. Am J Physiol Endocrinol Metab 2010;298:E1236–E1243
9. Minamiyama Y, Takemura S, Kodai S, et al. Iron restriction improves type 2 diabetes mellitus in Otsuka Long-Evans Tokushima fatty rats. Am J Physiol Endocrinol Metab 2010;298:E1140–E1149
10. Tajima S, Ikeda Y, Sawada K, et al. Iron reduction by deferoxamine leads to amelioration of adiposity via the regulation of oxidative stress and inflammation in obese and type 2 diabetes KKAy mice. Am J Physiol Endocrinol Metab 2012;302:E77–E86
11. Valenti L, Fracanzani AL, Dongiovanni P, et al. Iron depletion by phlebotomy improves insulin resistance in patients with nonalcoholic fatty liver disease and hyperferritinemia: evidence from a case-control study. Am J Gastroenterol 2007;102:1251–1258
12. Valenti L, Moscatiello S, Vanni E, et al. Venesection for non-alcoholic fatty liver disease unresponsive to lifestyle counseling–a propensity score-adjusted observational study. QJM 2011;104:141–149
13. Fernández-Real JM, Peñarroja G, Castro A, García-Bragado F, Hernández-Aguado I, Ricart W. Blood letting in high-ferritin type 2 diabetes: effects on insulin sensitivity and beta-cell function. Diabetes 2002;51:1000–1004
14. Ganz T. Macrophages and systemic iron homeostasis. J Innate Immun 2012;4:446–453
15. Corna G, Campana L, Pignatti E, et al. Polarization dictates iron handling by inflammatory and alternatively activated macrophages. Haematologica 2010;95:1814–1822
16. Recalcati S, Locati M, Marini A, et al. Differential regulation of iron homeostasis during human macrophage polarized activation. Eur J Immunol 2010;40:824–835
17. Orr JS, Puglisi MJ, Ellacott KL, Lumeng CN, Wasserman DH, Hasty AH. Toll-like receptor 4 deficiency promotes the alternative activation of adipose tissue macrophages. Diabetes 2012;61:2718–2727
18. Orr JS, Kennedy AJ, Hasty AH. Isolation of adipose tissue immune cells. J Vis Exp. 22 May 2013 [Epub ahead of print]
19. Kotecha N, Krutzik PO, Irish JM. Web-based analysis and publication of flow cytometry experiments. Curr Protoc Cytom 2010;Chapter 10;Unit10.17
20. Anderson EK, Hill AA, Hasty AH. Stearic acid accumulation in macrophages induces toll-like receptor 4/2-independent inflammation leading to endoplasmic reticulum stress-mediated apoptosis. Arterioscler Thromb Vasc Biol 2012;32:1687–1695
21. Livak KJ, Schmittgen TD. Analysis of relative gene expression data using real-time quantitative PCR and the 2(-Delta Delta C(T)) Method. Methods 2001;25:402–408
22. Asano Y, Meguro R, Odagiri S, Li C, Iwatsuki H, Shoumura K. Visualization of non-heme ferric and ferrous iron by highly sensitive non-heme iron histochemistry in the stress-induced acute gastric lesions in the rat. Histochem Cell Biol 2006;125:515–525
23. Lumeng CN, Bodzin JL, Saltiel AR. Obesity induces a phenotypic switch in adipose tissue macrophage polarization. J Clin Invest 2007;117:175–184
24. Nguyen KD, Qiu Y, Cui X, et al. Alternatively activated macrophages produce catecholamines to sustain adaptive thermogenesis. Nature 2011;480:104–108
25. Han J, Lee JE, Jin J, et al. The spatiotemporal development of adipose tissue. Development 2011;138:5027–5037
26. Cho CH, Koh YJ, Han J, et al. Angiogenic role of LYVE-1-positive macrophages in adipose tissue. Circ Res 2007;100:e47–e57
27. Zafon C, Lecube A, Simo R. Iron in obesity. An ancient micronutrient for a modern disease. Obes Rev 2010;11:322–328
28. Burgess A, Li M, Vanella L, et al. Adipocyte heme oxygenase-1 induction attenuates metabolic syndrome in both male and female obese mice. Hypertension 2010;56:1124–1130
29. Bekri S, Gual P, Anty R, et al. Increased adipose tissue expression of hepcidin in severe obesity is independent from diabetes and NASH. Gastroenterology 2006;131:788–796
30. Luciani N, Brasse-Lagnel C, Poli M, et al. Hemojuvelin: a new link between obesity and iron homeostasis. Obesity (Silver Spring) 2011;19:1545–1551
31. Boyle JJ, Johns M, Kampfer T, et al. Activating transcription factor 1 directs Mhem atheroprotective macrophages through coordinated iron handling and foam cell protection. Circ Res 2012;110:20–33
32. Kohyama M, Ise W, Edelson BT, et al. Role for Spi-C in the development of red pulp macrophages and splenic iron homeostasis. Nature 2009;457:318–321
33. Mantovani A, Sica A, Sozzani S, Allavena P, Vecchi A, Locati M. The chemokine system in diverse forms of macrophage activation and polarization. Trends Immunol 2004;25:677–686
34. Rumberger JM, Peters T Jr, Burrington C, Green A. Transferrin and iron contribute to the lipolytic effect of serum in isolated adipocytes. Diabetes 2004;53:2535–2541
35. Djeha A, Pérez-Arellano JL, Brock JH. Transferrin synthesis by mouse lymph node and peritoneal macrophages: iron content and effect on lymphocyte proliferation. Blood 1993;81:1046–1050
36. Davis RJ, Corvera S, Czech MP. Insulin stimulates cellular iron uptake and causes the redistribution of intracellular transferrin receptors to the plasma membrane. J Biol Chem 1986;261:8708–8711
37. Tanner LI, Lienhard GE. Insulin elicits a redistribution of transferrin receptors in 3T3-L1 adipocytes through an increase in the rate constant for receptor externalization. J Biol Chem 1987;262:8975–8980
38. Chung J, Kim MS, Han SN. Diet-induced obesity leads to decreased hepatic iron storage in mice. Nutr Res 2011;31:915–921
39. Le Guenno G, Chanséaume E, Ruivard M, Morio B, Mazur A. Study of iron metabolism disturbances in an animal model of insulin resistance. Diabetes Res Clin Pract 2007;77:363–370
40. Sonnweber T, Ress C, Nairz M, et al. High-fat diet causes iron deficiency via hepcidin-independent reduction of duodenal iron absorption. J Nutr Biochem 2012;23:1600–1608
41. Strissel KJ, Stancheva Z, Miyoshi H, et al. Adipocyte death, adipose tissue remodeling, and obesity complications. Diabetes 2007;56:2910–2918
42. Prieur X, Mok CY, Velagapudi VR, et al. Differential lipid partitioning between adipocytes and tissue macrophages modulates macrophage lipotoxicity and M2/M1 polarization in obese mice. Diabetes 2011;60:797–809